Bay of Bengal: Coupling of pre-monsoon tropical cyclones with the monsoon onset in Myanmar

Boniface O. Fosu[1] and S. -Y. Simon Wang[1, 2]

1. Department of Plants, Soils, and Climate, Utah State University, Logan, Utah

2. Utah Climate Center, Utah State University, Logan, Utah

Abstract

The pre-monsoon tropical cyclone (TC) activity and the monsoon evolution in the Bay of Bengal (BoB) are both influenced by the Madden Julian Oscillation (MJO), but the two do not always occur in unison. This study examines the conditions that allow the MJO to modulate the monsoon onset in Myanmar and TC activity concurrently. Using the APHRODITE gridded precipitation and the ERA-Interim reanalysis datasets, composite evolutions of monsoon rainfall and TC genesis are constructed for the period of 1979-2010. It is found that the MJO exhibits a strong interannual variability in terms of phase and intensity, which in some years modulate the conditions for BoB TCs to shortly precede or form concurrently with the monsoon onset in Myanmar. Such a modulation is absent in years of weaker MJO events in the vicinity of the BoB. Further understanding of the interannual variability of MJO activity could facilitate the prediction of the monsoon onset and TC formation in the BoB.

1. Introduction

The earliest onset of the South Asian summer monsoon (SASM) occurs in the Bay of Bengal (BoB) during May, followed consecutively by the onset over the South

China Sea and then over India (e.g., Lau and Yang 1998, Wu and Zhang 1998, Mao and Wu 2007). Together with the seasonal warming of sea surface temperature (SST), which peaks in May, formation of the monsoon trough in the BoB (Fig. 1a) provides favorable conditions not only for rainfall but also for tropical cyclones (TCs) (Wang et al. 2013). In contrast to other TC basins, the BoB experiences two distinctive peaks in the TC occurrence. The first TC season occurs in May before the SASM onset (pre-monsoon), and the second spans from October to November, after the monsoon (post-monsoon); this is shown in Fig. 1b in comparison to the seasonal rainfall in Myanmar. After the monsoon matures, prevailing low-level southwesterly winds and upper level easterly winds together create a strong vertical wind shear, and this is prohibitive for TC development. As a result, tropical disturbances that form at the heart of the monsoon season (Jun-Aug) seldom grow to become TCs, and instead, remain largely as monsoon depressions (Yoon and Huang 2012).

Within the seasonal changes, intraseasonal oscillations (ISOs) also affect monsoon development and TC formation in the BoB. The key conditions necessary for TC formation such as high SST, low vertical shear, and sufficient low-level vorticity (e.g., Gray 1979) are present in the BoB during spring. Although these features are important, it is also known that TCs do not form arise spontaneously simply because these conditions are met (Riehl 1948, Bergeron 1954, Rotunno and Emmanuel 1987). Instead, additional forcing such as ISO is needed to trigger tropical cyclogenesis (Emmanuel 2003, Krishnamohan et al. 2012). As was pointed out by Kikuchi and Wang (2010), about 60% of TCs over the Indian Ocean form in association with significant ISO events. Hereafter we refer to this process as “ISO-TC connection.”

The Madden-Julian Oscillation (MJO) is the largest intraseasonal fluctuation observed in the tropics (Madden and Julian 1971), and is responsible for a majority of weather variability (e.gs Jones et al. 2003, Molinari et al. 1997). The MJO is characterized by fluctuations of regional-scale deep convection and atmospheric divergent circulation; it exhibits a unique eastward propagation across the tropics within a period of about 30 to 60 days. An insightful review of the structure and physical mechanisms of the MJO is provided by Zhang (2005). Across the tropical oceans, the MJO can and does modify the large-scale circulation anomalies conducive for TC development, which is also the case in the BoB (e.g. Krishnamohan 2012, Kikuchi and Wang 2010). During the positive phase of the MJO (based on convergence over the Indian Ocean-western Pacific region), synoptic conditions that are favorable to TC development are considerably enhanced (Maloney and Hartmann 2000, Bessafi and Wheeler 2006, Ho et al. 2006). The MJO also influences the onset and intensity of the SASM, modulating the distinctive monsoon lifecycle that features alternating wet and dry spells known as break and revival periods (e.gs Goswami et al. 2003, Carvalho et al. 2004, Annamalai and Sperber 2005, Wheeler and Hendon 2004). While the positive phase of the MJO (enhanced convection) affects both the onset timing and intensity of the monsoon, the negative phase (suppressed convection) initiates breaks during the monsoon or can even prematurely end the monsoon (Lau and Waliser 2012, Wang 2006), including that in the BoB. Hereafter we refer to this as the "ISO-onset connection."

Even though SASM variability and TC development in the BoB have both been studied, the mechanism by which the MJO modulates the monsoon onset *and* TC activity collectively has not been explored. In other words, the relationship between the aforementioned ISO-onset and ISO-TC connections remains unclear – we refer to this as the "ISO-onset-TC connection," which is the goal of this study. In the following analyses, we show that certain (stronger) MJO events can provide unique conditions for pre-monsoon TCs in the BoB to shortly precede, or form concurrently with the monsoon onset, further enhancing rainfall in Myanmar.

Myanmar is highly vulnerable to the destructiveness of tropical cyclones, as is exemplified by tropical cyclone Nargis in May 2008, that caused catastrophic destruction with at least 130,000 reported fatalities (Webster 2008, McPhaden et al. 2009). Having only recently opened to the western world after years of civil unrest and political instability, Myanmar employs 65 percent of its active labor force in agriculture, an industry that is heavily reliant on monsoon and even TC rainfall. Wang et al. (2013) have reported an increase in the pre-monsoon TC activity in the BoB consisting of stronger TCs with eastward-tending tracks, and that such a change is due to increased anthropogenic aerosol loading in the atmosphere. Thus, additional understanding of the ISO-onset-TC connection will provide further insight into predicting the Myanmar monsoon onset and aid in disaster planning for TC impact.

This paper is organized as follows: section 2 briefly outlines the data used. In section 3, we introduce terminologies used throughout, and describe the analytical procedures utilized in the study. Results portraying the MJOs influence on the Myanmar monsoon onset and on BoB tropical cyclogeneses concurrently are discussed in section 4. Finally, a summary and conclusion are provided in section 5.

2. Data Sources

Four datasets are used in this study. The European Centre for Medium Range Forecasts reanalysis (Dee et al. 2011), available on a 1.5° by 1.5° latitude and longitude grid is used to derive streamfunction (Ψ), velocity potential (χ), and vertical wind shear (VWS), calculated from the difference in mean zonal (u) and meridional (v) winds between the 850 and 200-hPa pressure levels. For precipitation, the Asian Precipitation Highly-Resolved Observational Data Integration Towards Evaluation (APHRODITE) of Water Resources gridded precipitation dataset available on a 0.5° grid (Yatagai et al. 2012) is analyzed for the period of 1979 to 2010. Next, the National Center for Environmental Prediction (NCEP) sea surface temperature (SST) with a spatial resolution of about 1.875° by 1.875° (Kistler et al. 2001) is utilized, along with the NOAA outgoing longwave radiation (OLR) dataset. TC best track records are obtained from the Joint Typhoon Warning Center (JTWC) at their webpage (http://www.usno.navy.mil/NOOC/nmfc-ph/RSS/jtwc/best_tracks/ioindex.html).

3. Analysis procedures

Here we provide a description of analytical methods used. Interpretation and discussion of the results are presented in Section 4.

3.1 Onset definition

For the identification of yearly monsoon onset dates, we use western and central Myanmar (16^o-23^oN and 92^o-97^oE) for precipitation analysis, specified by the orange box in Fig. 1a. To define the monsoon onset, various meteorological parameters have been used with mixed results; these include wind speed and direction (Matsumoto 1992), precipitation (Matsumoto 1997, Wang and LinHo 2002), outgoing longwave radiation (Murakami and Matsumoto 1994) and cloud amount (Tanaka 1992). Among these parameters, rainfall is used operationally since its variation reflects the variability of the monsoon circulation system in general. According to Htway and Matsumoto (2011), the present definition of monsoon onset used by the Myanmar Department of Meteorology and Hydrology is the first day of three consecutive rainy days with daily rainfall amount of 2.54 mm or more. Yet, it is not uncommon to have three days of significant rainfall resulting from propagating tropical disturbances that may be unrelated to the development of monsoonal winds. It is therefore imperative to isolate such “bogus” onsets.

Against this backdrop, and knowing the monsoon exhibits a strong seasonal variability, we define a new onset selection scheme that can pick the yearly onset dates as representative as possible. The detailed procedure is as follows: first, we use the mean May precipitation to normalize the daily data, after which a 5-days running mean is applied. Beginning April 1, the onset criteria is satisfied on any day from which the accumulated rainfall of the preceding 14 days is less than the accumulated rainfall of the following 14 days. To ensure the difference between the two totals is substantial, as is expected for monsoon onsets, the difference must also be greater than a third of the total May precipitation. This procedure is illustrated in Fig. 2.

3.2 Composite evolutions for monsoon and TC

Using the selected onset dates, a composite evolution of monsoon rainfall is constructed based on the onset relative to each year. The evolution starts with the addition of precipitation 60 days prior to each onset and continues 40 additional days after, resulting in a 101-days composite evolution. This is demonstrated in Fig. 3a. Day 0 is the composite onset, or May 20 on average. Similar composites for circulation factors such as streamfunction (Ψ) at the 850-hPa level are displayed in Fig. 3b by averaging over longitude 80-100°E for 1) unfiltered fields (shaded), and 2) 30-60 days band passed fields (contours) to isolate the MJO signal. Tropical cyclogenesis days are then superimposed relative to the composite onset, at the specific latitude of their occurrence. Here, the day of TC genesis is defined by the first appearance as a tropical depression in the JTWC records. These results will be discussed along with Figs. 3 and 4.

Several studies have described Ψ and χ as more suitable for analyzing flow patterns when spatial scales are smaller than the Rossby radius of deformation (e.gs Palmer 1952, Li et al. 2006). Next, composites of Ψ and velocity potential (χ) are constructed based on the dates of tropical cyclogenesis. That way, we are able to depict the circulation features that promote TC genesis (Ventrice et al. 2013). In addition, onset based composites of χ, OLR and SST are also computed. To explicitly depict the MJO influences, we apply a 30-60 day bandpass filter on these fields. This bandpass window captures most Northern Hemisphere summer MJO variability. The results will be shown and discussed in Figs. 6 and 7. The year-to-year computation of Ψ is overlaid in Fig. 2 in comparison with each onset and TC occurrence.

3.3 EOF and regression analyses

Phase-space diagrams derived from Empirical Orthogonal Functions (EOFs) as described in Wheeler and Hendon (2004) can characterize the MJO's propagation and intensity with merely two parameters – phase and amplitude. A similar approach is used in this study. Several studies have used EOFs of single tropically confined fields that have been bandpass filtered to intraseasonal periods to identify the MJO (e.gs. Maloney and Hartmann 1998, Slingo et al. 1999, Matthews 2000, Kessler 2001). The first measure of the MJO we use here is based on bandpass filtered global velocity potential anomalies at 850-hPa. EOFs of bandpassed daily fields are computed from Apr 1 through June 30, and the corresponding principal components (PCs) of the first two modes are used to construct phase-space diagrams. The combination of the first two EOF's represents a half life cycle of the MJO, so when taken as a pair, the two PCs describe the global eastward-propagating signal attributed to the MJO. In order to gauge the strength of the MJO at any time, the PCs are normalized with their variances during the warm season. The EOFs would then exhibit two distinctive circulations signatures - the positive (wet) and negative (dry) phase. The positive phase of the MJO enhances rising motion and induces lower tropospheric convergence in the Indian Ocean-Western Pacific, whiles the negative phase suppresses rising motion. This result will be shown and discussed in Fig. 5.

Finally, using linear regression, the ENSO signal was removed from SST anomalies by subtracting from each grid point the regression coefficient of Niño 3.4 with SST from 1979 to 2010. The results are presented and discussed for Fig. 7d. A regression model is again used to illustrate the statistical relationship between SST variations in the BoB (5^o-20^oN and 80^o-89^oE, green boxes in Figs. 8 & 9) and ENSO. We analyze the mean response of BoB SST according to the magnitude and intervention of ENSO. These analyses will be discussed for Figs. 8 and 9.

4. Results and discussion

To explain the aforementioned three-way, "ISO-onset-TC connection" divulged in this study, we ought to first establish the relationship between the MJO and the Myanmar monsoon onset, i.e. the ISO-onset connection. Using methods outlined in section 3.2, the composite evolution of Myanmar monsoon rainfall is presented in Fig. 3a. Precipitation is persistently weak before the onset (day -60) until day 0 (or May 20) when an abrupt increase in rainfall occurs. About 15 days after the onset, a substantial decline in rainfall is observed (monsoon break). A comparison of the rainfall evolution with the latitude-time cross section of 850-hPa streamfunction (Ψ) anomalies (Fig. 3b) suggests the Myanmar monsoon onset (break) occurs during the positive (negative) phase of the MJO, represented by cyclonic (anticyclonic) circulation anomalies. This feature is consistent with the well-known northward migration of the 30-60 days mode and its modulation of the Indian summer monsoon.

Next, we investigate how the MJO influences TC formation and development in the BoB, i.e. the ISO-TC connection. The relationship between cyclogenesis and MJO evolution can be observed in Fig. 3b, where a majority of TCs occur within the MJO-enhanced monsoon trough. Furthermore, we plot TC genesis-based composites of the horizontal distribution of χ (Fig. 4a) and Ψ (Fig. 4b). In order to demonstrate how the MJO's migration relates to TC activity, the positions of each TC at the time of genesis (Day 0) and after (Day + 5 and Day +10) are shown. As seen in Fig. 4a, ten days before

TC genesis (Day -10), convergence associated with the MJO (positive phase) develops over the equatorial Western Indian Ocean. After five days (Day -5), the area of convergence shifts to India and the Indochina Peninsula. By the day of TC genesis (Day 0), the area of convergence exits India and moves farther east, centered over the Maritime continent. Five days after genesis, the MJO associated convergence crosses the maritime continent into the Western Pacific (Day +5), and travels farther east into the Eastern Pacific by the tenth day (Day +10). In terms of rotational flows (Fig. 4b), areas of cyclonic rotation (positive MJO phase) occur behind areas of convergence as the MJO propagates eastwards, this reflects the Gill-type dynamics. It is interesting but not surprising that TC genesis (Day 0) occurs with the strongest MJO trough in the BoB.

The results so far illustrates the ISO-onset (Fig. 3) and ISO-TC (Fig. 4) connections. However, as is noted in Fig. 3b, only 11 of the 27 pre-monsoon cyclogenesis occurred during or near the time of onset. This discrepancy suggests that, for the monsoon onset and TC genesis to occur concurrently (i.e. the ISO-onset-TC connection), additional environmental factors must be at play. To proceed, we first need to define TC-onset coupling: A “coupled” onset is one that occurs within 10 days (10 days before or after) of cyclogenesis in the BoB. There are 11 of such cases as outlined by the black box in Fig. 3b (*ref. Fig 2*), and these are referred to as “coupled TC-onset” cases. The rest of the onsets or TCs are considered “decoupled” cases. Since this paper targets the three-way Onset-ISO-TC, we limit the “decoupled” cases to only onsets that occurred within the positive phase of the MJO, without a TC occurrence within 10 days (or none at all). There are 13 of such ‘decoupled TC-onset’ cases.

Next, the amplitude and phasing of the MJO are examined through EOF analysis. Shown in Fig. 5a are the EOF1 patterns and their corresponding phase space diagrams for coupled TC-onset cases (in terms of years), abreast similar plots for decoupled TC-onset cases (Fig. 5b). The coupled cases generally boast stronger convergence/divergence patterns in EOF1 when compared to the decoupled cases (Fig. 5b) – this means the Indian Ocean-Western Pacific "mode" of MJO is strong. For ease of comparison, we add a black line that traces the center of convergence throughout all panels in the column. The line of track in Fig. 5a is clearly "straighter" than that in Fig. 5b, suggesting that the convergence center over the Indian Ocean-Western Pacific is more systematic and pronounced in the coupled cases, suggesting stronger MJO convergence during coupled TC-onsets, as opposed to decoupled events (Fig. 5b).

The shapes of the two sets of phase space diagrams are also noticeably different, indicating a difference in the phasing and propagation of the MJO. While many of the sequential days trace anti-clockwise, in eclipsed circles in the coupled cases (meaning EOF1 is distinctively stronger than EOF2), phase space diagrams of decoupled cases generally appear as round shaped circles ensuing from random motions of sequential days. Thus the coupled cases have persistent MJO cycles, with a stronger origin phase in the Indian Ocean-Western Pacific. The red dots in the MJO cycle indicate onsets, whiles the green dots show TC lifetime. In the coupled cases, monsoon onsets consistently occur during distinct MJO phases, while in the decoupled cases onsets mostly take place in weak MJO phases.

To explore further the TC-onset connection, we construct onset-based χ composites, which are presented in Fig. 6a for coupled cases and Fig. 6b for the decoupled cases. It again shows that in most cases, stronger (weaker) divergent circulations of the MJO accompany coupled (decoupled) cases. To facilitate comparison, a black parallel diagonal line is drawn connecting regions of maximum convergence to illustrate the MJO propagation for the coupled cases, shown in Fig. 6a; this line is then copied over to Figs. 6b and 6c. The difference between the phase and magnitude of the two groups is shown in Fig. 6c, indicating strong low-level convergence over the BoB 15 days prior to TC genesis, arguably pooling moisture and generating heat. There is seemingly a quarter-cycle phase difference between coupled and decoupled cases; this could mean that either the phase or the propagation speed is consistently different between the two cases. Such year-to-year differences in the phase and magnitude of the MJO may explain why the formation of BoB TCs is coupled with the Myanmar monsoon onset in some years but not in other years.

The synoptic conditions influencing onsets and TC geneses in the BoB are examined in Fig. 7, which shows the differences (coupled - decoupled) in the composite vertical wind shear (VWS), streamfunction (Ψ), outgoing longwave radiation (OLR) and SST. Prior to the coupled onsets, vertical wind shear weakens (Fig. 7a). Likewise, the BoB monsoon trough deepens (Fig. 7b) and surface convection intensifies (Fig. 7c), forming conditions conducive for TC formation. Within the low-level convergence phase of the MJO (Day-15 through Day 0; *ref.* Fig. 4b), equatorial westerlies intensify and subsequently enhance cyclonic circulation over the BoB (Fig. 7b). Meanwhile, an upper-level anticyclone develops (not shown) resulting in a reduction in vertical wind shear, which is favorable for TC development (e.g., Gray 1968, Zehr, 1992, DeMaria and Kaplan 1999). After the monsoon onset, VWS increases and an anticyclone anomaly moves from the equator replacing the cyclonic anomaly, suppressing convection while creating unfavorable conditions for TC formation over the BoB. The timescale of these variations are reminiscent of the MJO as well as its modulation on TC activity.

Also noteworthy is the SST variation associated with the TC-onset coupling, as is shown in Fig. 7d. Warmer waters develop prior to and during the onset (and TC genesis). This means increased energy fluxes towards the development of the monsoon trough that favors TC formation. Although the SST variation hints of an MJO modulation, SST in the BoB always maintains a critical temperature of above 27^{o}C that is needed for tropical cyclogenesis, so its role might be secondary. Nonetheless, further SST warming in the BoB does create feedbacks with evaporation and convection while enhancing low-level convergence (*ref.*, Fig. 4a). This leads to destabilization of the lower troposphere resulting in a rapid intensification of the BoB monsoon trough (Fig. 7b). Yet, there is an apparent SST cooling after the onset, presumably due to the post-onset and/or TC rainfall that cool the ocean surface (note that the ENSO signal in SST has been linearly regressed out).

The observed intraseasonal variation in SST is an intriguing feature. Previous studies have shown that intraseasonal SST variations do provide feedback to the MJO and vice versa (e.gs Wang and Xie 1998, Waliser et al. 1999). Thus, we examine the relationship between the BoB SST (averaged between, 5^{o}-20^{o}N and 80^{o}-89^{o}E, green box in Fig. 8) and global SST through a composite approach. We analyze the winter (DJF) and pre-monsoon (MAM) seasons for 1) years in which the onset and TCs were coupled (Fig. 8) and 2) years in which the onset and TCs were not coupled (Fig. 9). For coupled cases, there is a discernable but rather weak ENSO signal in both seasons, while the BoB SST is consistently warmer (Fig. 8). However, for decoupled cases (Fig. 9) the BoB SST is cooler and yet the ENSO signal is robust. Given the removal of the ENSO signal, and our earlier analysis showing that a stronger MJO and warmer SST favors the coupled cases, the results from Figs. 8 and 9 suggest that the MJO tends to be stronger in the Indian Ocean-Western Pacific during moderate ENSO events and weaker during strong ENSO events. This finding is consistent with the observations by Hendon et al (1998) that the overall level of MJO activity is found to be uncorrelated with El Nino except during exceptionally warm ENSO events by which the MJO is suppressed. A further analysis of the BoB SST using EOF (not shown) reveals that, while EOF2 produces a SST pattern resembling that in the coupled TC-onset cases, it only explained 17% of the variance. Correlation of PC2 with global SST suggested that there is no significant El Nino influence. It is therefore inferred that the subseasonal variability in SST revealed from Fig. 7d is mostly a response to the MJO's propagation; this also implies that much of the yearly MJO variability may be internally generated.

Finally, we note that the composite monsoon break as shown in Fig. 3b occurs within the negative phase of the MJO. It appears unfavorable conditions associated with this phase of the MJO may be an influencing factor in suppressing rainfall.

5. Concluding remarks

We have examined the extent to which the MJO modulates springtime TCs in the BoB, the Myanmar monsoon onset, and eventually their coupling (or occurrence) in certain ways. The monsoon onset tends to initiate during the positive phase of the MJO (trough in the BoB) while the monsoon break occurs during the negative phase (ridge in the BoB). TCs in the BoB also tend to form during the positive phase of the MJO. When the MJO's positive phase coincides with the seasonal development of the monsoon trough during strong MJO activity seasons, TC genesis and monsoon onset are likely to occur concurrently. The MJO activity exhibits a marked interannual variability, which can be explained by a combination of magnitude and phasing, from which the concurrence of TC geneses and monsoon onsets are both controlled. Given the relative strengths of MJO events in both coupled and decoupled cases, and how sensitive cyclogeneses are to environmental conditions, it seems plausible to say that it is the phasing of the MJO that more predominantly modulates the coupling. As the low-level convergence of the MJO propagates through the BoB, the cyclonic anomaly develops and leads to a rapid intensification of westerlies and influx of moisture into the BoB. This leads to the intensification of the BoB monsoon trough. In the meantime, vertical wind shear is reduced, thus providing a favorable environment for TCs to form.

The SST in the BoB reaches its seasonal maximum around 30^{o} in spring. The warm SST amplifies the MJO modulation on TC geneses through feedbacks of evaporation and convection, and provides moisture for sustaining convection. The BoB SST anomaly was not found to link significantly with the interannual variability of the MJO. However, we did find that the MJO tends to intensify during weak/moderate El Nino events, and weaken during strong El Nino events.

Dynamical predictions of the Asian summer monsoon have advanced significantly in recent decades. Previous studies that analyzed retrospective predictions of the NCEP Climate Forecast System have indicated that the model could simulate the broad structure of the Asian monsoon (Saha et al. 2006, Yang et al. 2008, Gao et al.

2011, Drbohlav and Krishnamurthy 2010). However, some key features are missing in the hindcasts such as the shifts of the maximum precipitation from the equator to around 15^oN (Jiang et al. 2012). Looking forward, the results of this study can provide further information to augment current predictions techniques of the monsoon during the spring and early summer season, especially for the monsoon onset over Myanmar.

Acknowledgements

We would like to thank Robert Gillies and Brendan Buckley for their insightful suggestions. This study was supported by the United States Agency for International Development grant EEM-A-00-383 10-00001 and the NASA Grant NNX13AC37G, and approved by the Utah State University Agricultural 384 Experimental Station.

References

Annamalai H, Sperber KR (2005) Regional heat sources and the active and break phases of boreal summer intraseasonal (30-50 day) variability. J Atmos Sci 62:2726-2748.

Bergeron T (1954) The problem of tropical hurricanes. Q J R Meteorol Soc 80:131-64

Bessafi M, and Wheeler MC (2006) Modulation of south Indian Ocean tropical cyclones by the Madden–Julian oscillation and convectively coupled equatorial waves. Mon Wea Rev 134:638-656.

Carvalho LMV, Charles J, Tércio A (2005) Opposite Phases of the Antarctic Oscillation and Relationships with Intraseasonal to Interannual Activity in the Tropics during the Austral Summer. J Clim 18:702-718.

Dee DP et al (2011) The ERA-Interim reanalysis: configuration and performance of the data assimilation system. Q J R Meteorol Soc 137:553-597. doi: 10.1002/qj.828.

DeMaria M, Kaplan J (1999) An updated statistical hurricane intensity prediction scheme (SHIPS) for the Atlantic and eastern North Pacific basins. Weather Forecast 14:326-37.

Drbohlav HK, Krishnamurthy V (2010) Spatial structure, forecast errors, and predictability of the South Asian monsoon in CFS monthly retrospective forecasts. J Clim 23:4750-4769

Emanuel KA (2003) Tropical cyclones. Annu Rev Earth Planet Sci 31:75-104

Emanuel KA (1987) The dependence of hurricane intensity on climate. Nature 326:483 85

Gao H, Yang S, Kumar A, Hu Z-Z, Huang B, Li Y, and Jha B (2011) Variations of the East Asian mei-yu and simulation and prediction by the NCEP Climate Forecast System. J Clim 24:94-108.

Goswami BN, Mohan RA, Xavier PK, Sengupta D (2003) Clustering of low pressure systems during the Indian summer monsoon by intraseasonal oscillations. Geophys Res Lett 30:8. doi: 10.1029/2002GL016,734.

Gray WM (1968) Global view of the origin of tropical disturbances and storms. Mon Weather Rev 96:669-700.

Gray WM (1979) Hurricanes: Their formation, structure and likely role in the general circulation. In: Shaw DB (ed) Meteorology over the Tropical Oceans. Royal Meteorological Society, J Glaisher House, Grenville Place, Bracknell, Berks, pp155-218.

Guard CP, Carr LE, Wells FH, Jeffries RA, Gural ND, Edson DK (1992) Joint Typhoon Warning Center and the Challenges of Multi basin Tropical Cyclone Forecasting. Wea Forecasting 7:328-352.

Hendon HH, Zhang C, Glick JD (1999), Interannual variation of the Madden-Julian Oscillation during Austral summer. J Clim 12: 2538-2550.

Ho CH, Kim JH, Jeong JH, Kim HS, Chen D (2006) Variation of tropical cyclone activity in the south Indian Ocean: El Niño–Southern Oscillation and Madden–Julian oscillation effects. J Geophys Res 111:D22101. doi:10.1029/2006JD007289.

Jiang X, Yang S, Li Y, Kumar A, Liu X, Zuo Z, and Jha B (2012) Seasonal-to-interannual prediction of the Asian summer monsoon in the NCEP Climate Forecast System Version 2. J Clim. doi:10.1175/JCLI-D-12-00437.1.

Jones C, Carvalho LMV, Wayne HR, Waliser DE, Schemm KE (2004) A statistical forecast model of tropical intraseasonal convective anomalies. J Clim 17:2078-2095.

Kikuchi K, Wang B (2010) Formation of tropical cyclones in the northern Indian Ocean associated with two types of tropical intraseasonal oscillation modes. J Meteorol Soc Jpn 88:475-496

Kistler R et al (2001) The NCEP–NCAR 50–Year Reanalysis: Monthly Means CD–ROM and Documentation. Bull Amer Meteor Soc 82:247-267.

Krishnamohan KS, Mohankumar K, Joseph PV (2012) The influence of Madden–Julian oscillation in the genesis of North Indian Ocean cyclones. Theor Appl Climatol 109:271-282. doi:10.1007/s00704-011-0582-x

Li Z, Yi C, McWilliams JC (2006) Computation of the Streamfunction and Velocity Potential for Limited and Irregular Domains. Mon Wea Rev 134:3384-3394.

Madden RA, Julian PR (1971) Detection of a 40-50 day oscillation in the zonal wind in the tropical Pacific. J Atmos Sci 28:702-708.

Maloney ED, Hartmann DL (2000) Modulation of eastern North Pacific hurricane by the Madden–Julian oscillation. J Clim 13:1451-1460.

Mao JY, Wu GX (2007) Interannual variability in the onset of the summer monsoon over eastern Bay of Bengal. Theor Appl Climatol 89:155-170.

Matsumoto J (1992) The seasonal changes in Asian and Australian monsoon regions. J Meteorol Soc Jpn 70:257-273.

Matsumoto J (1997) Seasonal transition of summer rainy season over Indochina and adjacent monsoon region. Adv Atmos Sci 14(2):231-245.

McPhaden MJ et al (2009) Ocean-atmosphere interactions during cyclone Nargis. EOS, Transactions, AGU, 90:53-60.

Molinari J, Knight MD, Vollaro D, Skubis S (1997) Potential vorticity, easterly waves, and tropical cyclogenesis. Mon Wea Rev 125:2699-2708.

Monaldo FM, Sikora TD, Babin SM, Sterner RE (1997) Satellite Imagery of Sea Surface Temperature Cooling in the Wake of Hurricane Edouard. Mon Wea Rev 125:2716-2721.

Murakami T, Matsumoto J (1994) Summer monsoon over the Asian continent and Western North Pacific. J Meteorol Soc of Jpn 72(5):719-745.

Palmer CE (1952) Tropical meteorology. Quart J Roy Meteorol Soc 78:126-164

Riehl H (1950) A model for hurricane formation. J Appl Phys 21:917-25.

Saha S et al (2006) The NCEP Climate Forecast System. J Clim 19:3483-3517.

Salby ML, Hendon HH (1994) Intraseasonal behavior of clouds, temperature, and winds in the Tropics. J Atmos Sci 51:2207-2224.

Tanaka M (1992) Intraseasonal oscillation and the onset and retreat dates of the summer monsoon over East, Southeast Asia and the Western Pacific region using GMS high cloud amount data. J Meteorol Soc of Jpn 70 (1): 613–629.

Ventrice MJ, Wheeler MC, Hendon HH, Schreck CJ, Thorncroft CD, Kiladis GN (2013) A modified multivariate Madden-Julian oscillation index using velocity potential. Mon Wea Rev 141:12, 4197-4210.

Waliser DE (2005) Predictability and forecasting. In: Lau WKM, Waliser DE (eds) Intraseasonal Variability of the Atmosphere-Ocean Climate System. Springer, Heidelberg, Germany, pp 389-423.

Waliser DE, Lau KM, Kim J-H 1999b: The influence of coupled sea surface temperatures on the Madden-Julian Oscillation: A model perturbation experiment. J Atmos Sci 56: 333-358.

Wang B, LinHo (2002) Season of the Asian-Pacific summer monsoon. J Clim 15:386-398.

Wang B (ed) 2006: The Asian Monsoon. Springer-Praxis, pp 787.

Wang B, Xie X (1998) Coupled Modes of the Warm Pool Climate System. Part I: The Role of Air–Sea Interaction in Maintaining Madden–Julian Oscillation. J Clim 11:2116-2135.

Wang S-Y, B. Buckley BM, Yoon JH, Fosu BO (2013) Intensification of premonsoon tropical cyclones in the Bay of Bengal and its impacts on Myanmar. J Geophys Res Atmos 118:4373-4384. doi:10.1002/jgrd.50396.

Webster PJ (2008) Myanmar's deadly daffodil. Nature Geoscience. 488-490.

Wheeler MC, Hendon HH (2004) An all-season real-time multivariate MJO index: Development of an index for monitoring and prediction. Mon Weather Rev 132:1917-1932.

Wu GX, Zhang YS (1998) Tibetan Plateau forcing and the timing of the monsoon onset over South Asia and the South China Sea. Mon Wea Rev 126:913-927.

Wu G, Guan Y, Liu Y, Yan J, Mao J (2012) Air–sea interaction and formation of the Asian summer monsoon onset vortex over the Bay of Bengal. Clim Dyn 38:261-279.

Yang S, Lau K-M (1998) Influences of sea surface temperature and ground wetness on Asian summer monsoon. J Clim 11:3230-3246.

Yang S, Zhang Z, Kousky VE, Higgins RW, Yoo S-H, Liang J, Fan Y (2008) Simulations and seasonal prediction of the Asian summer monsoon in the NCEP Climate Forecast System. J Clim 21:3755-3775.

Yatagai et al(2012) APHRODITE: Constructing a Long-Term Daily Gridded Precipitation Dataset for Asia Based on a Dense Network of Rain Gauges. Bull Amer Meteor Soc 93:1401-1415.

Yoon JH, Huang WRJ (2012) Indian Monsoon Depression. In: Wang S-Y, Gillies RR (eds) Modern Climatology, InTech, Rijeka, Croatia, pp 45-71.

Zehr RM (1992) Tropical cyclogenesis in the western North Pacific. In NOAA Tech. Rep. NESDIS 61, pp 181.

Zhang C (2005) Madden-Julian Oscillation. Rev Geophys. doi:10.1029/2004RG000158

Figure

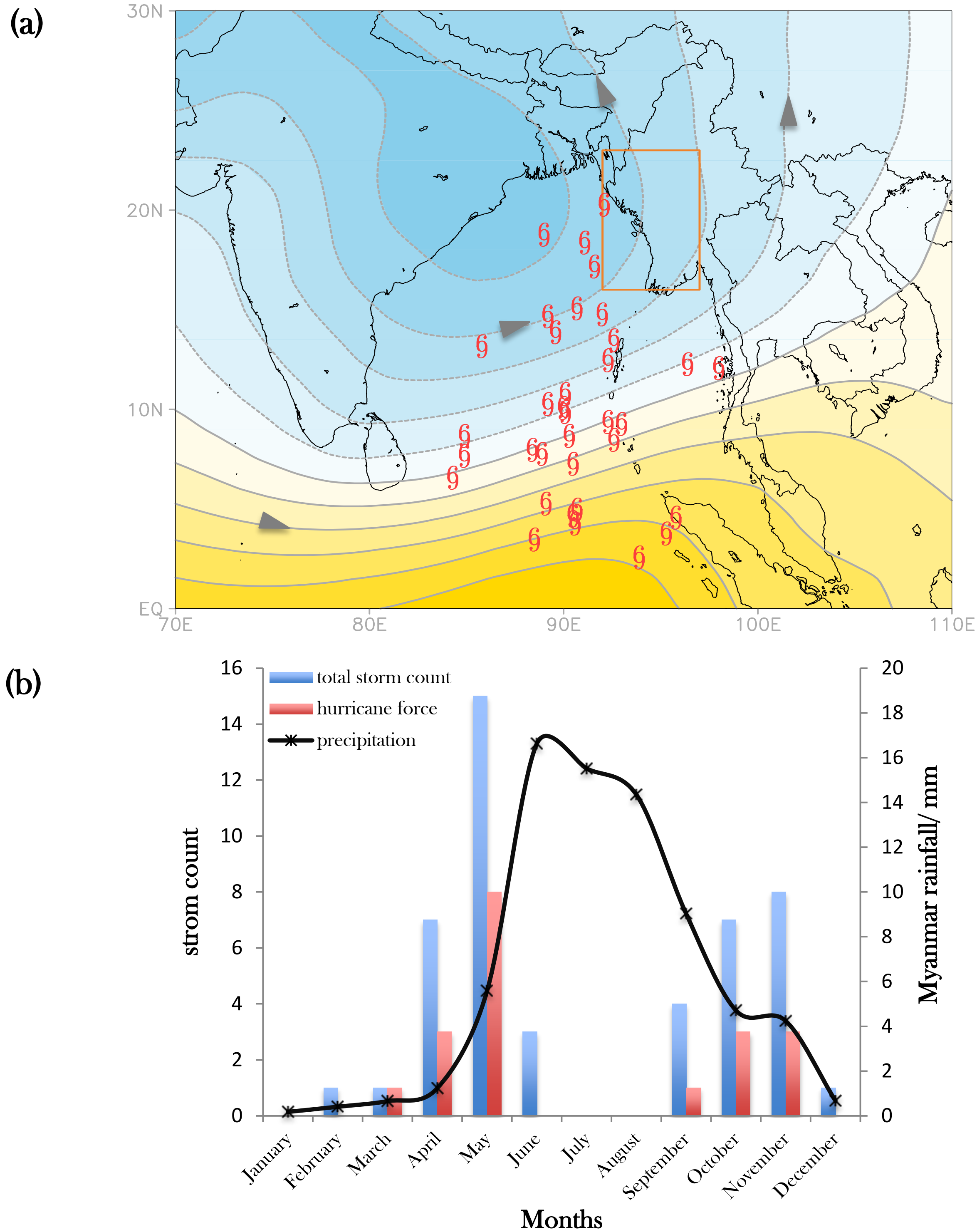

Fig. 1

a Mean 850-mb streamfunction (Ψ) (contour interval: 1.2 $10^6 m^2 s^{-1}$) of May, overlaid with all post 1979 spring cyclogenesis locations (red typhoon symbols) in the BoB. **b** Tropical storm count in the BoB and rainfall distribution averaged from the orange box in **a** (western and central Myanmar). Hurricane force storms (red TC symbols) are cyclones with wind speeds greater than 107 km/h.

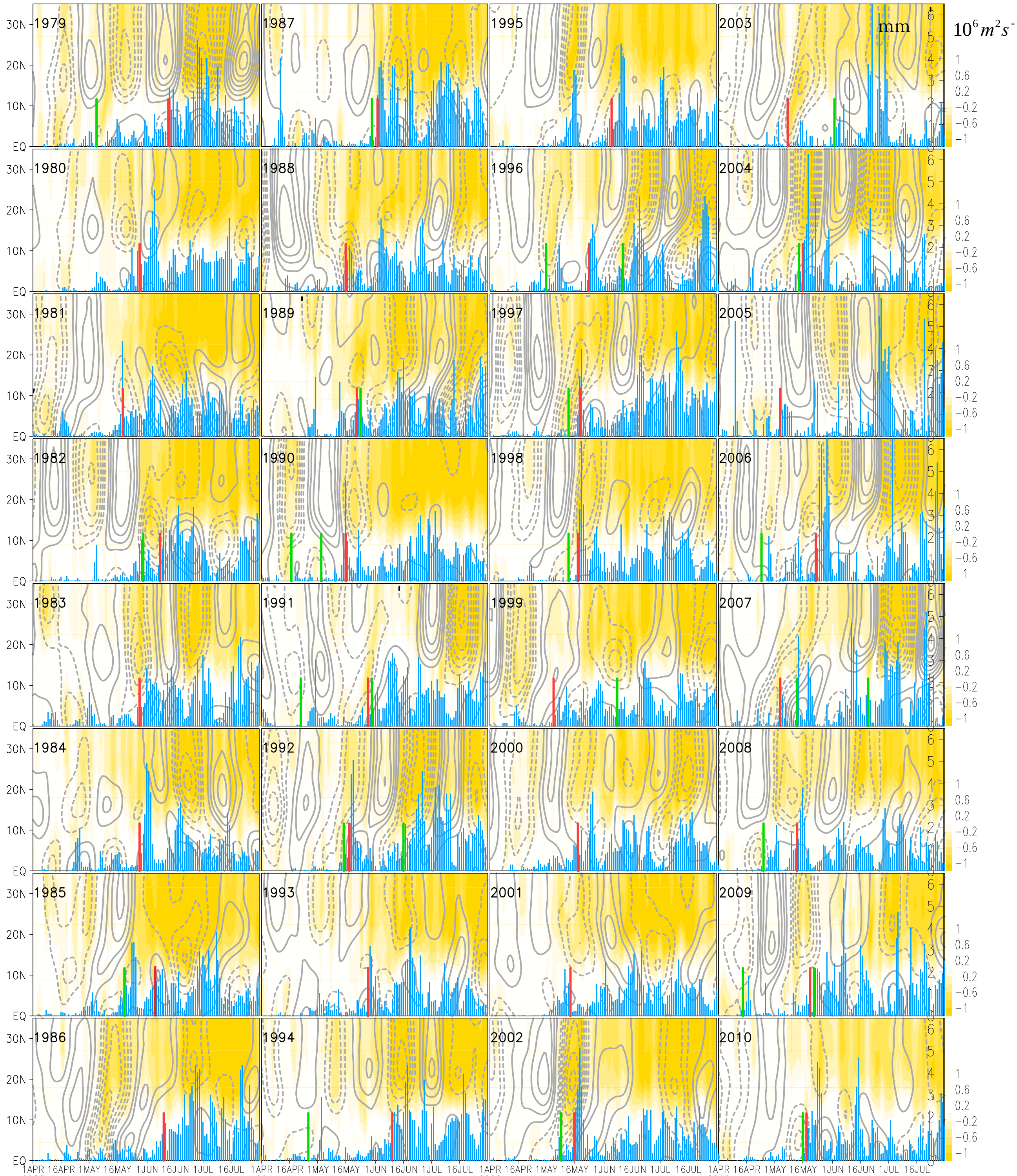

Fig. 2

850-hPa unfiltered Ψ fields (shaded), superimposed with 30-60 days bandpassed Ψ (contours, interval: $0.7 10^6 m^2 s^{-1}$) averaged over longitude 80-100 E. Histograms of daily precipitation from April through July over western and central Myanmar for each year is overlaid in blue. Red and green lines show onset and tropical cyclogenesis dates respectively.

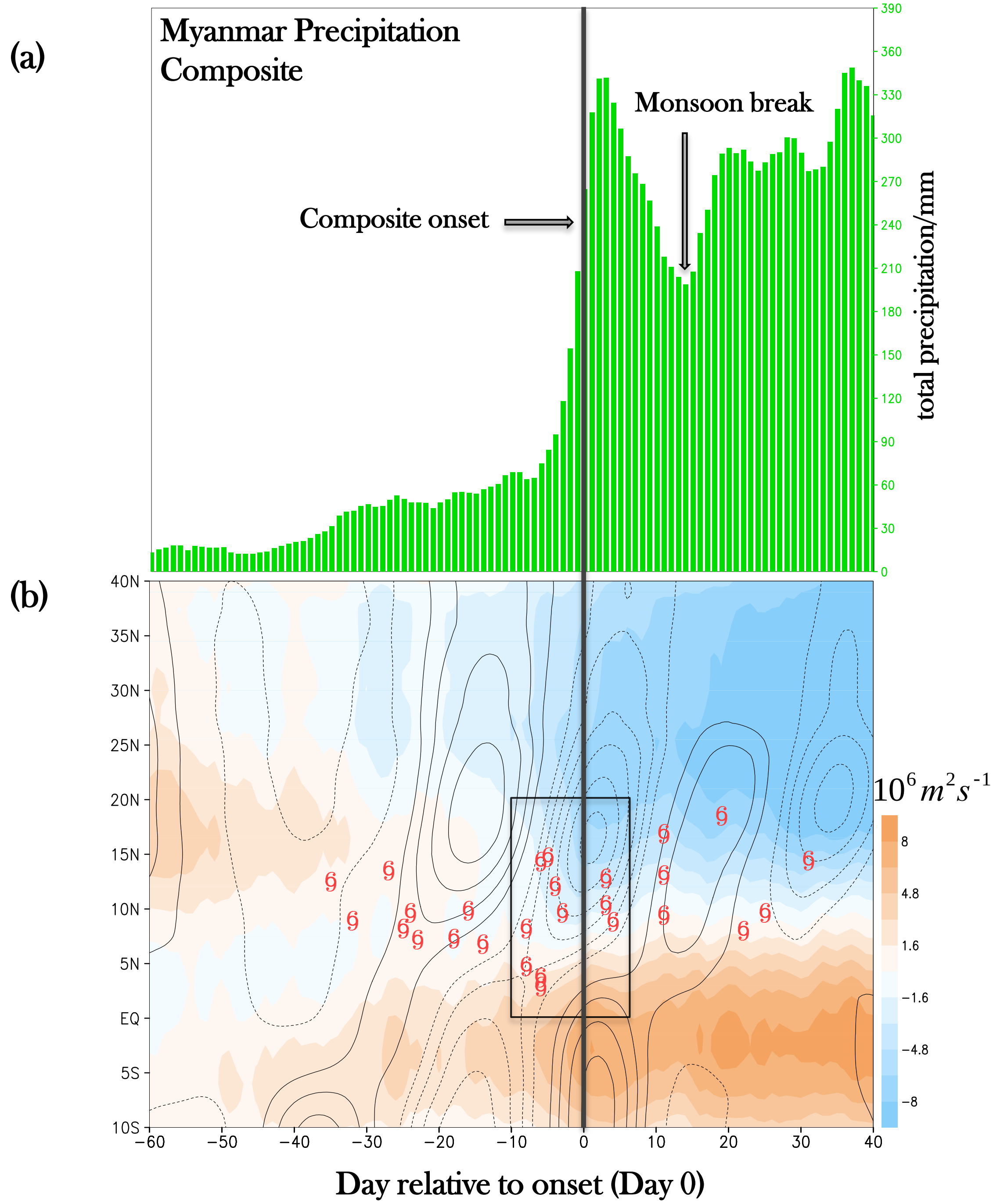

Fig. 3

a Composite evolution of daily rainfall averaged over western and central Myanmar. The average onset is May 20 (day 0, black line). **b** Composite evolution of 850-hPa unfiltered Ψ fields (shaded), superimposed with 30-60 days bandpassed Ψ (contours, interval:1.6 $10^6 m^2 s^{-1}$) averaged over longitude 80-100 E with the locations of all pre-monsoon tropical cyclogenesis (red TC symbols) superimposed. Cyclogenesis days are plotted relative to the composite onset, at the same latitude they occurred. The black box indicates where the definition of coupled TC-onset cases is made.

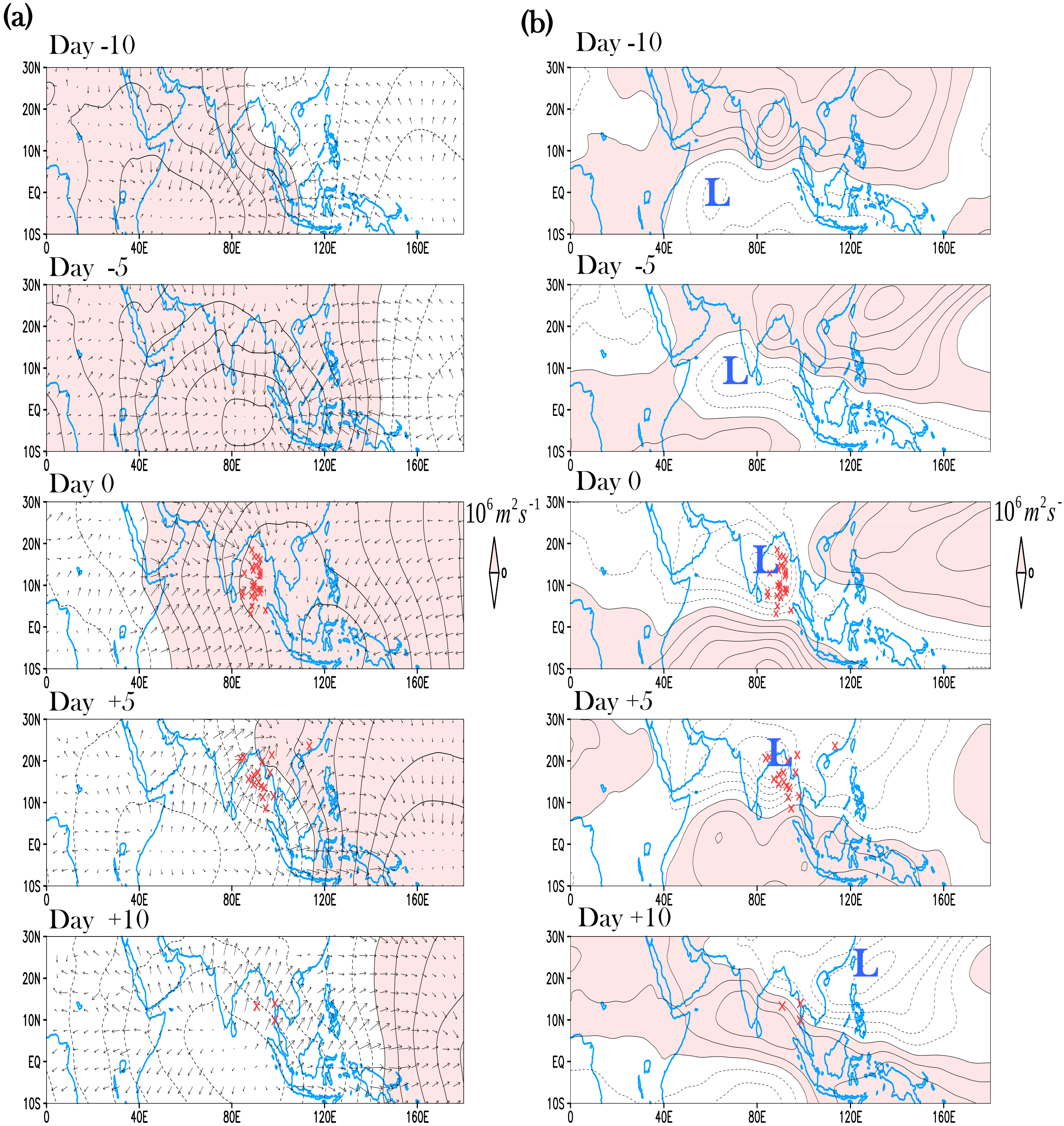

Fig. 4

Composites 850-hPa **a** χ and **b** Ψ based on 27 post 1979 pre-monsoon cyclogenesis, applied with a 30-60 day bandpass filtering (contour interval: 0.3 $10^6 m^2 s^{-1}$). Vectors in **a** represent divergent winds while positive anomalies are shaded. Places marked with **"L"** in **b** show the center of the trough. The position of each TC at the time of genesis to 10 days after are also superimposed using red multiplication marks.

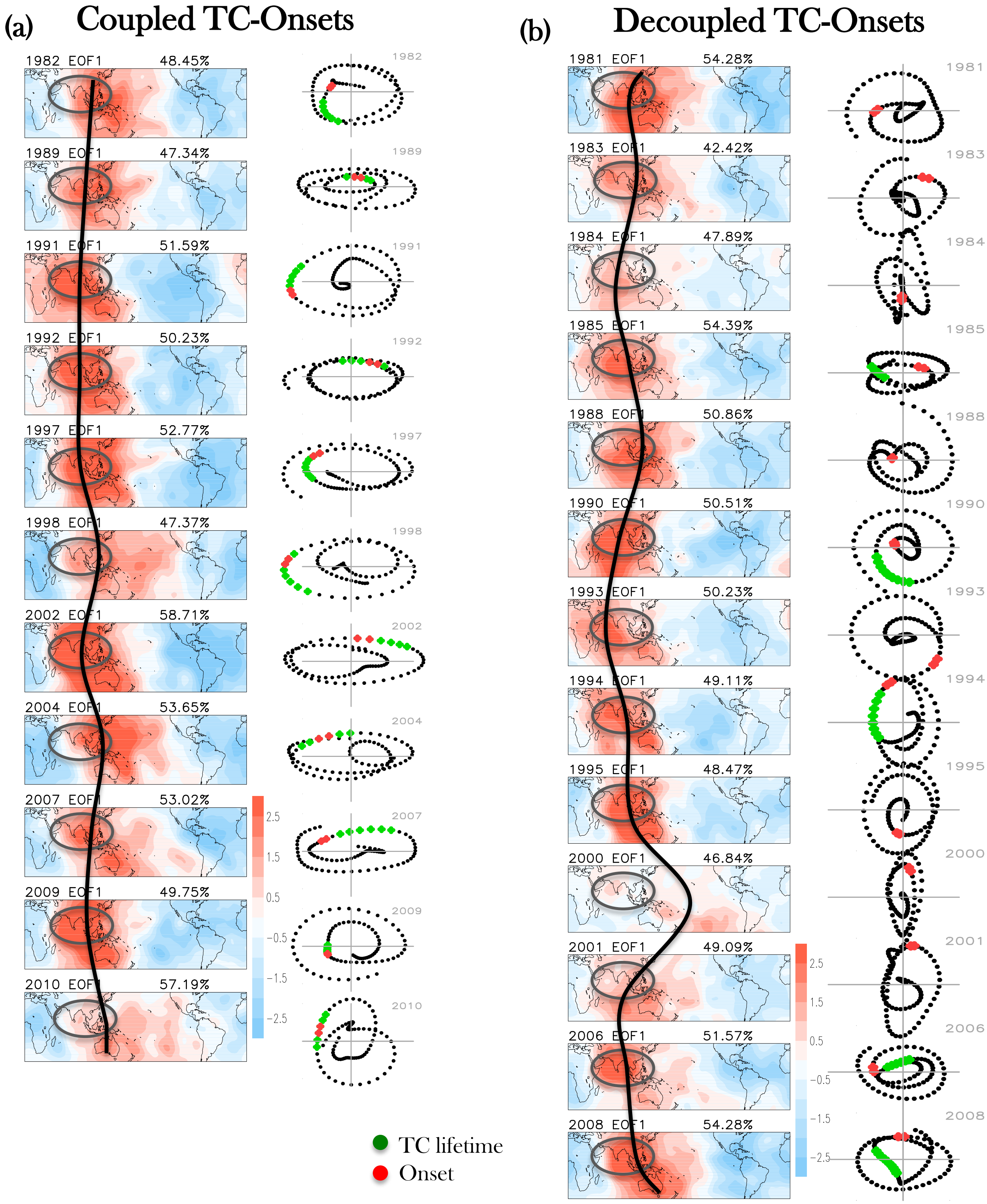

Fig. 5

EOFs of 30-60 days bandpassed χ at 850-hPa for **a** coupled TC-onset cases and **b** decoupled TC-onset cases, along with phase space from April through June, using PC1 and PC2. The black lines join centers of enhanced convergence. The red dots show the onset whiles the green dots show TC lifetime. Circles mark NIO.

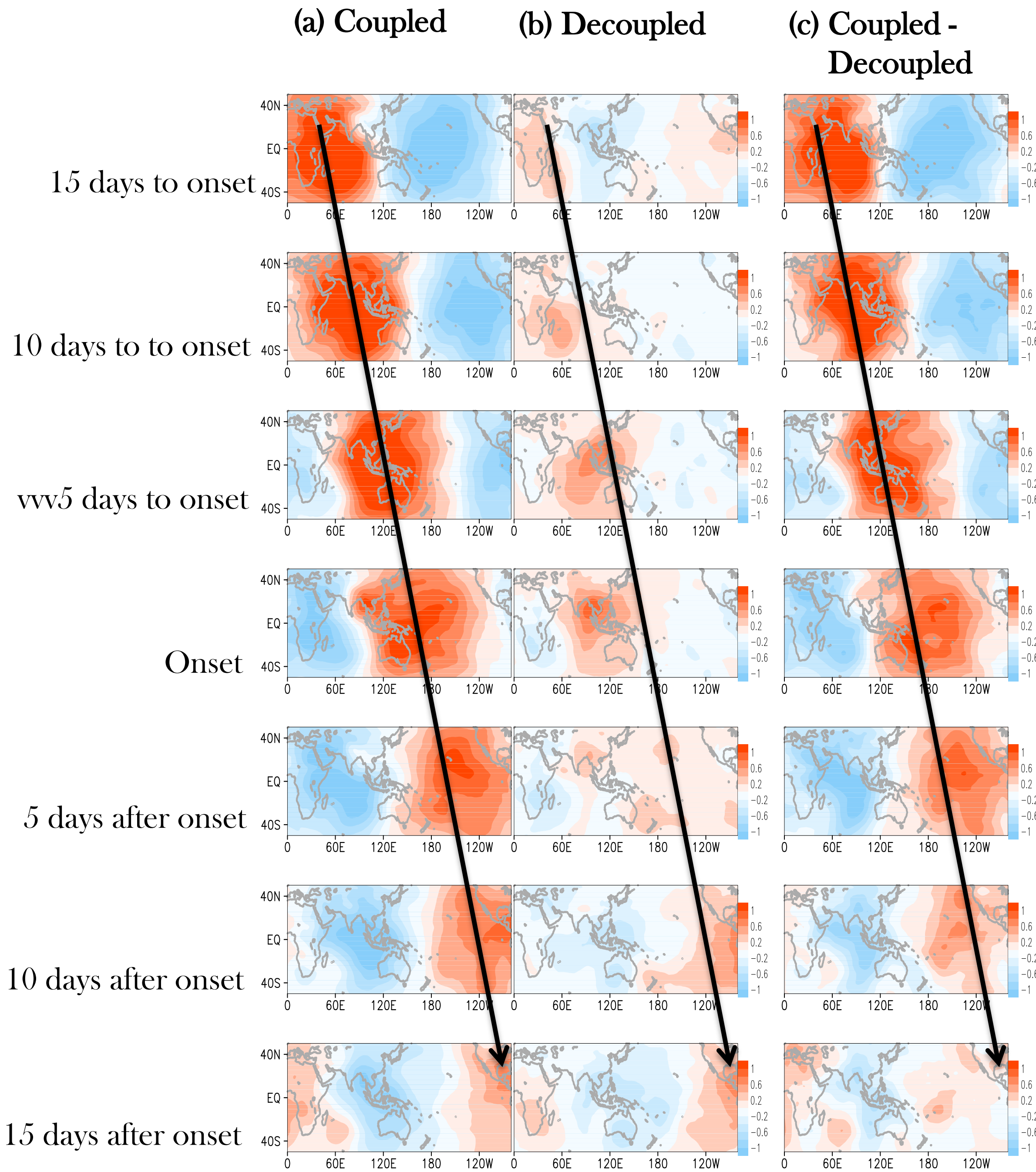

Fig. 6

Mean composites of 850-hPa 30-60 bandpassed χ based on **a** coupled TC-onset cases, **b** decoupled cases, and **c** difference between the two groups. The black parallel lines runs across the same region on the maps in each case.

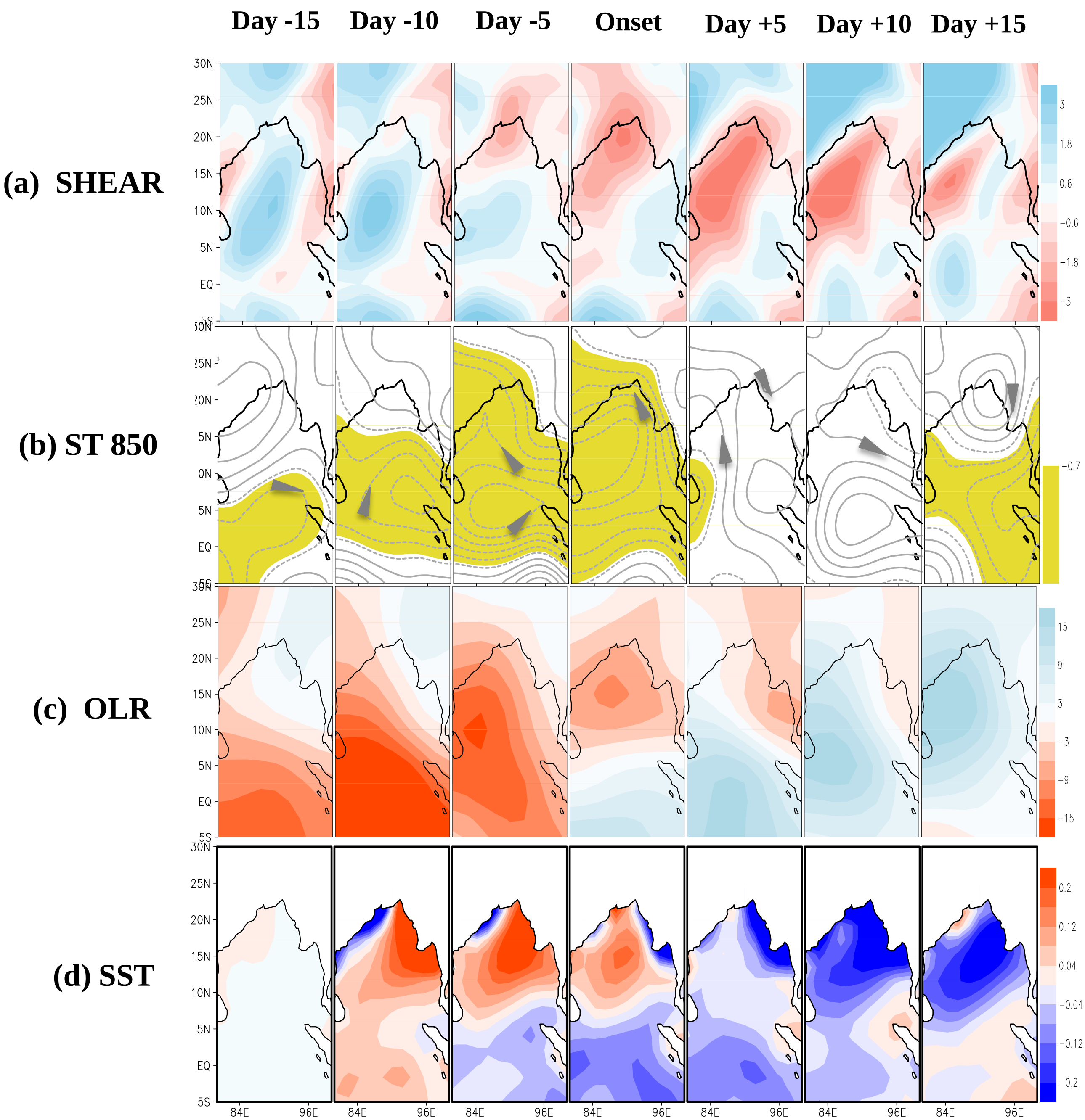

Fig. 7

Horizontal maps showing differences in **a** VWS (m/s), **b** 30-60 days bandpassed Ψ at 850-hP ($10^6 m^2 s^{-1}$) , **c** OLR (Wm^{-2}) and **d** SST (K) ; between mean composites of **a** coupled cases, and **b** decoupled cases (coupled –decoupled). ENSO signal is removed from SST composites.

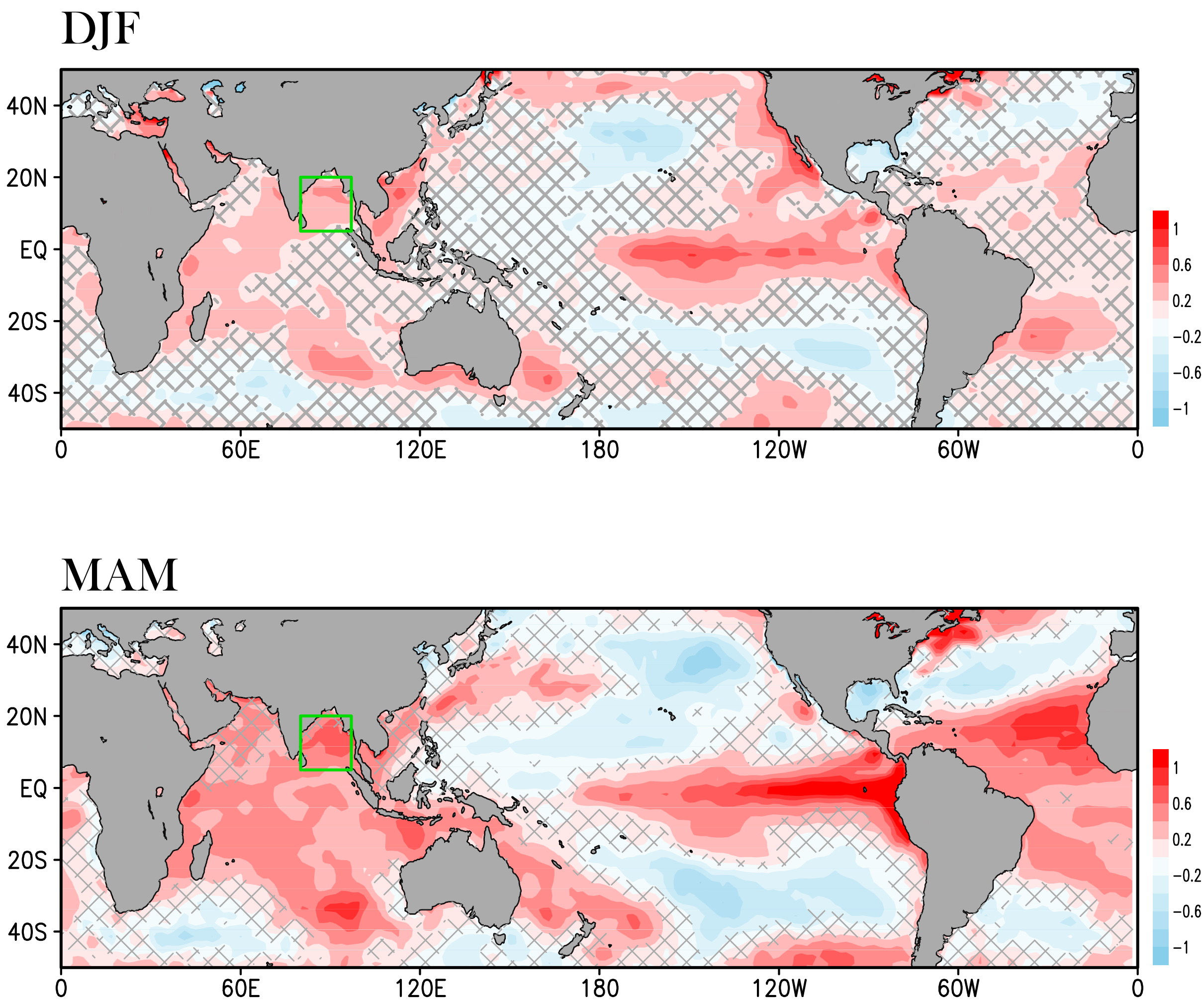

Fig. 8

Global SST regressed with BoB SST based on coupled TC-onset cases (i.e. a composite approach). Only coupled years are used. The green box in the BoB outlines the domain used (longitude $80 - 97^o E$ and latitude $5 - 20^o N$). The grey mesh masks out insignificant areas (confidence interval = 95%).

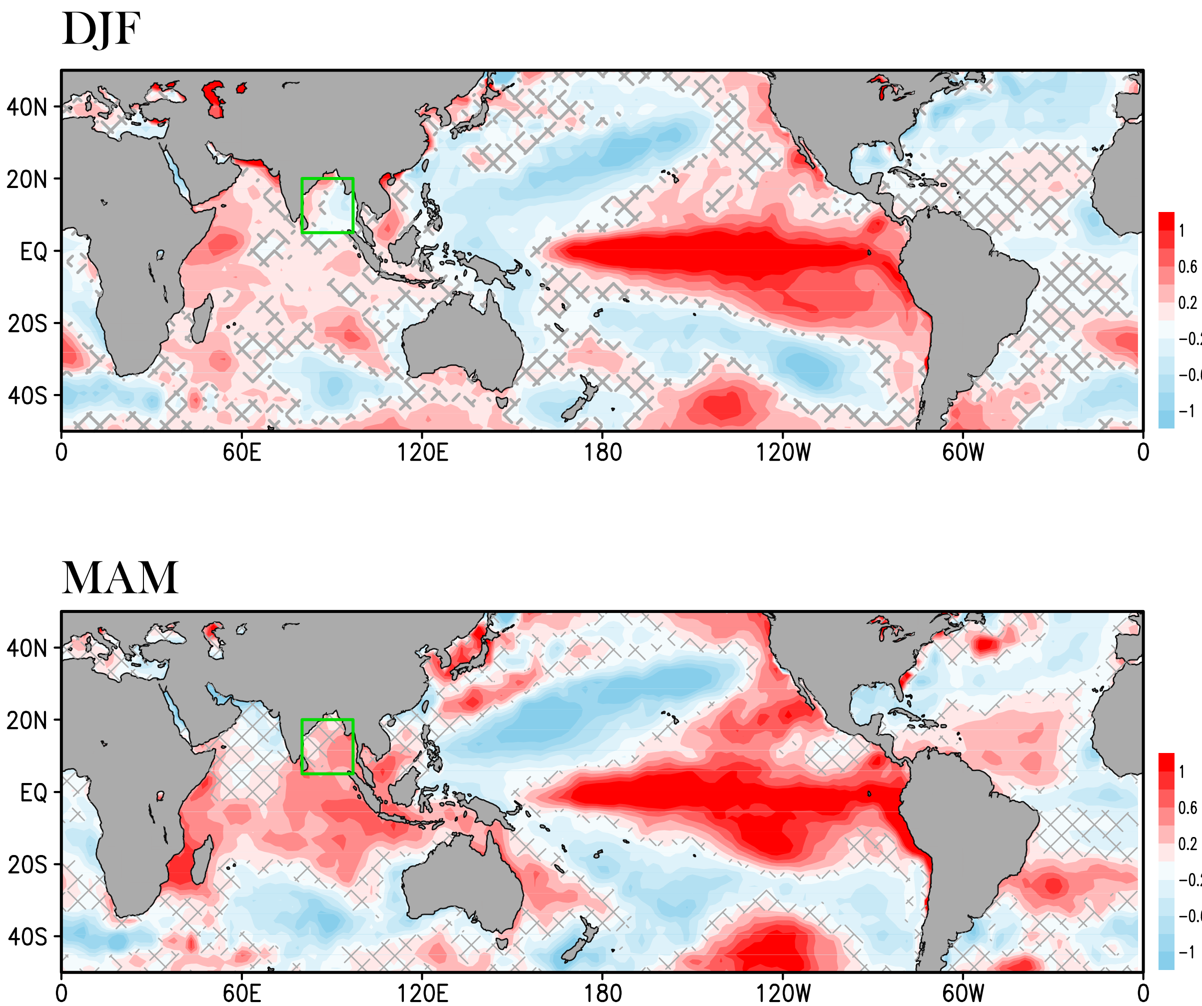

Fig. 9

Same as Fig. 8 but for decoupled TC-onset cases. Only decoupled years are used.